Differential method applied for photonic crystals

Evgeny Popov and Bozhan Bozhkov

The classic differential method is applied for modeling the diffraction of light from two-dimensional photonic crystals that consist of dielectric cylindrical objects. Special attention is paid to mutual interpenetration of consecutive layers. Two algorithms for dealing with a stack of repetitive layers are discussed, namely, the eigenvalue technique and the *S*-matrix algorithm. Their advantages and limitations are analyzed, and times required for their implementation are compared. © 2000 Optical Society of America

OCIS codes: 050.1940, 050.1960.

1. Introduction

The past 15 years have brought into the fore a new class of materials called photonic crystals,[1–3] mainly because of the formation of a bandgap (thus, crystals) in the transmittivity of light (thus, photonic). Although their behavior is quite similar to that of the well-known bandgap multilayer optical coatings, photonic crystals have more dimensions (two-dimensional or three-dimensional geometry), which extends their almost perfect reflectivity in a given optical region to a much wider angular interval,[4] sometimes a complete sphere.

The first theoretical studies of these materials used solid-state physical methods and an analogy between Helmholtz and Maxwell equations.[5,6] However, propagation of light in the so-called resonance domain (wavelength of the same order of magnitude as the characteristic distance between the constituent particles) obeys some rules that have made the scalar approach irrelevant. Strong polarization dependencies of both the propagation equation and the boundary conditions, the possibility of guided and surface wave excitation, and cutoff anomalies are among the factors that have led to the relative failure of the approximate (scalar or vectoral) approaches to model light diffraction by periodic structures, in particular, by diffraction gratings.[7]

The authors are with the Institute of Solid State Physics, Bulgarian Academy of Sciences, 72 Tzarigradsko Chaussee Boulevard, Sofia 1784, Bulgaria. The e-mail address for E. Popov is popov@mbox.cit.bg.

Received 7 January 2000; revised manuscript received 13 June 2000.

0003-6935/00/274926-07$15.00/0

Several rigorous approaches to light scattering by two-dimensional periodic structures were developed recently. Some are based on a single-object scattering matrix, which is used to characterize the diffraction by each crystal component and thus to form the total system response.[8] However, this approach requires that the objects not interpenetrate, i.e., that there be circles that enclose the components without intersecting. Other approaches are independent of the elements' forms but require that there be no interpenetration among different layers of cylinders.[9,10] A recent review of theoretical methods that were used to model photonic crystal diffraction can be found in Ref. 11 and the references cited therein.

In this paper we propose a modification of the differential method that is capable of dealing with any two-dimensional array, with or without penetration (Fig. 1). Whereas recent hybridization of the differential method with the so-called *R*- (or *S*-) matrix propagation algorithm[12] is, in principle, suitable for treating such systems, numerical integration throughout the entire stack would need computation times proportional to the entire system thickness. Here we propose a method that uses the fact that there are (numerous, but not infinite) identical layers in the vertical direction. This new formulation leads to numerically stable results with a computation time that is independent of the total thickness of the system. One can use the computer code based on this method to evaluate the reflectivity of a stack of any number (100, 5000, or more) of identical layers with the same amount of computational effort (and of time). For example, for identical layers of dielectric cylinders the time for calculation of a single diffraction could be less than 1 s on a PC, based on a 300-MHz Pentium II processor, in TE polarization, increasing to a 1 m for TM polarization or for inclusion of metallic compo-

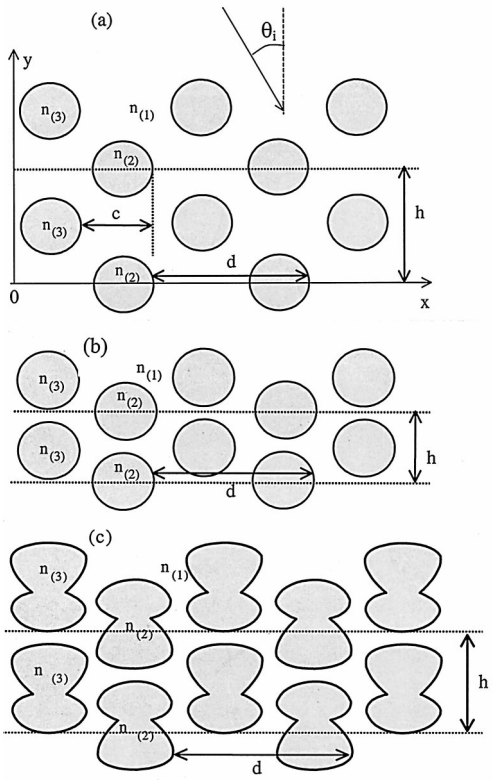

Fig. 1. Schematic representation of three scattering systems consisting of cylindrical objects.

nents. In Section 3 we present such examples, after formulating the method in Section 2.

2. Differential Method for a System of Identical Multilayers

The diffraction system under consideration is shown schematically in Fig. 1. It must be pointed out that, if such a system could be divided into slices separated by homogeneous layers [e.g., cylinders without interpenetration; Fig. 1b], the integral method[7,9] could be applied quite successfully. However, the mutual penetration of the objects in the vertical direction limits the application of the plane-wave expansion (the Rayleigh hypothesis[7,13]) in the interpenetration region, which greatly complicates application of the integral method.[14] The differential method, however, can easily permit artificial system slicing, even if the slice boundary intersects the physical object boundaries, but at the cost of a slower convergence rate in TM polarization for highly conducting objects.

Below and above the entire diffraction system the scattered (and incident) light components can be represented as a plane-wave expansion (Rayleigh components):

$$F_z^{(j)}(x,y) = \sum_n \{b_n^{(j+)}\exp[i\beta_n^{(j)}y] + b_n^{(j-)}\exp[-i\beta_n^{(j)}y]\}\exp(i\alpha_n x),$$
$$F_x^{(j)}(x,y) = \sum_n iq^{(j)}\beta_n^{(j)}\{b_n^{(j+)}\exp[i\beta_n^{(j)}y] - b_n^{(j-)}\exp[-i\beta_n^{(j)}y]\}\exp(i\alpha_n x), \quad (1)$$

with $j = 0$ corresponding to the substrate and $j = N$ to the cladding. In TE polarization $F_z = E_z$ is equal to the z component of electric vector $\mathbf{E}$ and $F_x = \omega\mu_0 H_x$ is equal to the normalized x component of magnetic vector $\mathbf{H}$. Depending on the polarization, the coefficient $q^{(i)}$ is equal to

$$q^{(j)} = \begin{cases} 1 & \text{TE} \\ 1/k^2 n_{(j)}^2 & \text{TM} \end{cases}, \quad (2)$$

where $k = 2\pi/\lambda$ is the vacuum wave number, λ is the wavelength, and $n_{(j)}$ is the jth medium's refractive index. Horizontal and vertical wave-vector components α and β are defined by the relations

$$\alpha_m = \alpha_0 + mK, \quad \beta_m^{(j)2} = k^2 n_{(j)}^2 - \alpha_m^2. \quad (3)$$

Here

$$K = 2\pi/d, \quad (4)$$

where d is the distance between the cylinders in the x direction (i.e., the grating period), and

$$\alpha_0 = kn_{(N)}\sin\theta_0^{(N)} \quad (5)$$

is directly linked to angle of incidence $\theta_0^{(N)}$ in the cladding medium.

Here we use the classic differential formalism[7,12] to evaluate the reflected and transmitted amplitudes, but this formalism could be any that crosses the profile (the horizontal lines in Fig. 1 cross the interfaces of the objects) such as the method of Moharam and Gaylord.[15] In contrast, methods that parallel the profile (as is the case with the integral method[7]) cannot be used directly when there is interpenetration of the scattering objects, as we discussed in Section 1.

For self-consistency, we present the basic equations briefly, so the interested reader should be able to understand the algorithm without other references. Because of the rigorous periodicity of the system in the x direction, the field components are quasi-periodic with respect to x, and the Floquet theorem can be applied:

TE polarization

$$E_z(x,y) = \sum_m E_m(y)\exp(i\alpha_m x), \quad (6)$$

$$H_x(x,y) = \frac{1}{\omega\mu_0}\sum_m H_m(y)\exp(i\alpha_m x). \quad (7)$$

TM polarization

$$H_z(x,y) = \frac{1}{\omega\mu_0}\sum_m H_m(y)\exp(i\alpha_m x), \quad (8)$$

$$E_x(x,y) = -\sum_m E_m(y)\exp(i\alpha_m x). \quad (9)$$

The denominator $\omega\mu_0$ in Eq. (8) is introduced for convenience.

The partial-derivative Maxwell equations can be

written as a set of first-order differential equations in TE polarization:

$$\frac{\mathrm{d}E_n(y)}{\mathrm{d}y} = iH_n(y),$$
$$\frac{\mathrm{d}H_n(y)}{\mathrm{d}y} = -i\alpha_n^2 E_n(y) + i\sum_m \Im_{n-m}(y)E_m(y), \quad (10)$$

and in TM polarization:

$$\frac{\mathrm{d}H_n(y)}{\mathrm{d}y} = i\sum_m \Im_{n-m}(y)E_m(y),$$
$$\frac{\mathrm{d}E_n(y)}{\mathrm{d}y} = iH_n(y) - i\alpha_n \sum_m \Re_{n-m}(y)\alpha_m H_m(y), \quad (11)$$

where $\Im_n(y)$ are the Fourier components of k^2n^2 and

$$\Re(x,y) = \sum_m \Re_m(y)\exp\left(im\frac{2\pi}{d}x\right) \equiv \frac{1}{k^2 n_{(j)}^2(x,y)}. \quad (12)$$

Numerical integration of Eqs. (10) or (11) from one level of $y = y_j$ to $y_{j+1} = y_j + h$ could be made by use of the elementary solutions as starting elements:

TE case

$$\tilde{E}_{np}^{\pm}(y_j) = \delta_{np},$$
$$\tilde{H}_{np}^{\pm}(y_j) \equiv \pm i\left.\frac{\mathrm{d}\tilde{E}_{np}^{\pm}}{\mathrm{d}y}\right|_{y=y_j} = \pm\beta_n^{(1)}\delta_{np}, \quad (13)$$

TM case

$$\tilde{H}_{np}^{\pm}(y_j) = \delta_{np},$$
$$\tilde{E}_{np}^{\pm}(y_j) = \pm\frac{1}{k^2 n_{(1)}^2}\beta_n^{(1)}\delta_{np}, \quad (14)$$

a choice that ensures the continuity of the tangential field components at $y = y_j$ with the nth component $\exp[i\alpha_n x \pm i\beta_n^{(1)}y]$ of Rayleigh expansion in Eq. (1). In fact, we assume that the system is separated into slices along the dotted lines (Fig. 1), yielding intermediate infinitely thin layers with optical indices of $n_{(1)}$. This can be done because field components F_z and F_x are continuous across these artificial interfaces.

The result of numerical integration of the field components enables us to obtain the amplitudes of the Rayleigh expansion $b^{(j+1)}$ at the artificial cut $y = y_{j+1}$ as a linear combination of amplitudes $b^{(j)}$ at $y = y_j$:

$$\begin{bmatrix} b_n^{(j+1,+)} \\ b_n^{(j+1,-)} \end{bmatrix} = \begin{bmatrix} T_{11}^{(j)} & T_{12}^{(j)} \\ T_{21}^{(j)} & T_{22}^{(j)} \end{bmatrix} \begin{bmatrix} b_n^{(j,+)} \\ b_n^{(j,-)} \end{bmatrix}. \quad (15)$$

The matrix

$$T^{(j)} = \begin{bmatrix} T_{11}^{(j)} & T_{12}^{(j)} \\ T_{21}^{(j)} & T_{22}^{(j)} \end{bmatrix} \quad (16)$$

is called a transmission matrix of the jth slice and is obtained from the result of numerical integration at $y = y_{j+1}$:

$$\begin{matrix} T_{11}^{(j)} \\ T_{12}^{(j)} \\ T_{21}^{(j)} \\ T_{22}^{(j)} \end{matrix} \begin{bmatrix} \tilde{E}_{nm}^{+}(y_{j+1}) + \tilde{H}_{nm}^{+}(y_{j+1})/q^{(1)}\beta_m^{(1)} \\ \tilde{E}_{nm}^{-}(y_{j+1}) + \tilde{H}_{nm}^{-}(y_{j+1})/q^{(1)}\beta_m^{(1)} \\ \tilde{E}_{nm}^{+}(y_{j+1}) - \tilde{H}_{nm}^{+}(y_{j+1})/q^{(1)}\beta_m^{(1)} \\ \tilde{E}_{nm}^{-}(y_{j+1}) - \tilde{H}_{nm}^{-}(y_{j+1})/q^{(1)}\beta_m^{(1)} \end{bmatrix}. \quad (17)$$

Let us imagine that the scattering system consists of identical slices numbered from 1 to $N-2$. The first slice, for example, the lower half of the first layer of cylinders, could be different from the others. The same could be valid for slice $N-1$ (e.g., the upper part of the last cylinders). The link between the amplitudes of the Rayleigh expansion in the substrate ($j = 0$) and in the cladding ($j = N$) is given through the transmission matrix T of the entire system, which is a product of the transmission matrices of the various slices:

$$T = T^{(N-1)}[T^{(j)}]^{N-3}T^{(1)}. \quad (18)$$

Moreover, if N is large, it is not necessary to make multiple multiplications of matrices to raise the power of $T^{(j)}$. We can do this by decomposing $T^{(j)}$ into eigenvectors and eigenvalues:

$$T^{(j)} = V\Phi W, \quad (19)$$

where V is the matrix that contains in its columns the eigenvectors of $T^{(j)}$, $W = V^{-1}$, and Φ is a diagonal matrix with its elements the corresponding eigenvalues γ of $T^{(j)}$. The pth power of $T(j)$ requires merely the raising of the Mth diagonal elements to a power of p:

$$\lfloor T^{(j)} \rfloor^p = V\Phi^p W, \quad (20)$$

this decomposition requires many fewer matrix operations and is much faster.

However, it is well known that integration (direct or not) of a thick system exhibits numerical instabilities as a result of growing exponential terms that correspond to evanescent diffraction orders inside the system. There are several ways to avoid this problem. Probably the most promising one is the so-called S- (from scattering) or R- (from reaction, originating from chemistry) matrix algorithm, which is discussed in Section 3. First we want to point out where the instabilities come in the transmission [T-matrix approach] and how to overcome them by regrouping the terms in Eq. (20). The main advantage of this algorithm is that it requires equal computation times, independently of the system's thickness (i.e., of the number of layers N). However, there is a limit to this approach when the thickness of each slice (which forms the photonic crystal lattice in the y direction) becomes large enough. This problem is discussed at the end of this section.

Experience shows that the eigenvalues of T vary across a large number of magnitudes. This fact can be easily understood when one is investigating the

transmission matrix for a homogeneous layer. The logarithm of eigenvalues γ is equal to $i\beta^{(j)}h$, because they give the y dependence of the field components. However, as far as the field consists of downward- and upward-propagating space harmonics, then $\gamma_n = \exp(\pm i\beta_n h)$ and there are growing and evanescent terms with complex values of β. When the imaginary part of β multiplied by the slice's thickness has a large enough modulus, there are large exponential terms, which lead to numerical truncation of the physically important propagating terms (with β real). These arguments could be applied directly for a modulated (nonhomogeneous) slice, for which the index modulation does not depend on the vertical direction, e.g., lamellar or phase gratings with straight vertical grooves. It can easily be shown that, if γ_n is an eigenvalue, $1/\gamma_n$ is also an eigenvalue; i.e., again small- and large-magnitude eigenvalues coexist.

A multilayered system increases the problems because each eigenvalue in Eq. (20) is raised to a positive-integer (number of layers) power. To avoid this numerical underflow of physically important terms compared with growing exponentially components, one can separate the eigenvalues into two groups: large, $\Phi_1 = \{\gamma_n\}$:Re[log(γ_n)] ≥ 0, and small, $\Phi_2 = \{\gamma_n\}$:Re[log(γ_n)] ≤ 0. Eigenvector matrix V and its inverse W must be represented in block form after rearrangement according to the order of eigenvalues (large and small):

$$V = \begin{bmatrix} V_{11} & V_{12} \\ V_{21} & V_{22} \end{bmatrix}, \qquad W = \begin{bmatrix} W_{11} & W_{12} \\ W_{21} & W_{22} \end{bmatrix}. \tag{21}$$

After trivial calculation and assuming that there is no incidence from the substrate side, it can be shown that the entire transmission matrix of the system takes the form

$$T = \begin{bmatrix} T_{11}^{(N-1)} & T_{12}^{(N-1)} \\ T_{21}^{(N-1)} & T_{22}^{(N-1)} \end{bmatrix} \begin{pmatrix} V_{11} + V_{12}Q \\ V_{11} + V_{12}Q \end{pmatrix} [W_{11}T_{12}^{(1)} + W_{12}T_{22}^{(1)}], \tag{22}$$

where

$$Q_{mn} = (\Phi_{2m}/\Phi_{1n})^{N-3}\{[W_{21}T_{12}^{(1)} + W_{22}T_{22}^{(1)}] \times [W_{11}T_{12}^{(1)} + W_{12}T_{22}^{(1)}]^{-1}\}_{mn}. \tag{23}$$

It is obvious that the growing terms arise in Q and remain in the denominator. Thus they never affect the numerical stability. The exceptions are discussed later in this section.

The result is that the method can successfully treat multilayer systems with arbitrary numbers of layers. As an example, we consider a case already presented in the literature.[9] There is no interpenetration, so the case could be treated with the integral method. The spectral dependencies are presented in Fig. 2 for several numbers of cylinder layers: 15 ($N = 7$), 31 ($N = 15$), and 201 ($N = 100$). The results for the first case (15 cylinder layers) are identical to those given in Ref. 9. The computation time for each point of the curves is ~1 s on a 300-MHz Pentium II-based PC, independently of the number of layers. The truncation (M) of the matrices is set to seven diffraction orders.

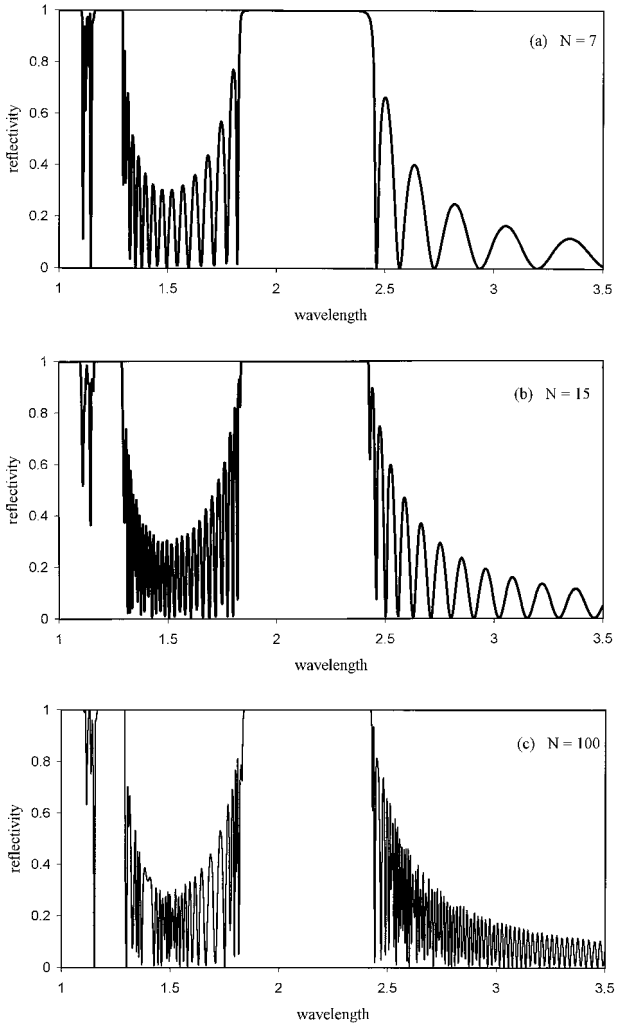

Fig. 2. Reflectivity of a system without penetration and various numbers of layers. Identical cylinders with radius 0.2 μm; horizontal distance, $d = 1$ μm; $c = 0.5$ μm; vertical distance, $h = 1.73205$ μm (i.e., cylinders lie in the corners of equilateral triangles), $n_1 = 1$, $n_2 = n_3 = 2$, normal incidence, TE polarization. (a) $N = 7$ (i.e., the total number of rod layers is 15), (b) $N = 15$, (c) $N = 100$.

However, the simple hypothesis of symmetrical behavior of the eigenvalues, which ensures the good numerical behavior of matrix Q, holds only for low-truncation parameter M. Whereas this value could be used for dielectric rods in TE polarization, increasing the optical index of the rods (real and imaginary parts) or working in TM polarization requires an increase in the value of M. Then the eigenvalues of the single-slice transmission matrix become large (Table 1), so the elements of matrix Q all become zero, even for a few layers N. Fortunately, in that case we can use the well-known S-matrix algorithm,[16] which substitutes scattering matrix S for transmission matrix T. However, to go from one slice to the upper slice it is necessary to use a recurrent link instead of power dependence, as was done for Eq. (23). Thus

Table 1. Eigenvalues of the Transmission Matrix for Two Values of Truncation Parameter M[a]

$M = 7$		$M = 13$	
Re(log γ)	Im(log γ)	Re(log γ)	Im(log γ)
31.49927585	$0.1258217411 \times 10^{-19}$	64.72334287	$-0.3041395378 \times 10^{-19}$
31.46402818	$-0.607743150 \times 10^{-20}$	64.71407837	$0.3037544383 \times 10^{-19}$
20.04158652	$0.7502387872 \times 10^{-18}$	53.72054093	$0.9754650566 \times 10^{-19}$
19.87065245	$-0.6603937882 \times 10^{-18}$	53.71132825	$-0.8024249290 \times 10^{-19}$
6.949721305	$0.4511018174 \times 10^{-17}$	42.65543473	$-0.3873075109 \times 10^{-19}$
6.078492698	$-0.6709885795 \times 10^{-17}$	42.65401497	$0.4736915901 \times 10^{-19}$
-0.41969×10^{-6}	−2.902894289	31.48935089	$-0.5735529253 \times 10^{-18}$
-0.41969×10^{-6}	2.902894289	31.45055608	$0.2336299143 \times 10^{-18}$
−5.706233657	$-0.1591353641 \times 10^{-13}$	27.77626336	3.141592654
−6.076166756	$0.6355391827 \times 10^{-14}$	21.02603800	$0.1333590748 \times 10^{-11}$
−6.457099755	−3.141592654	19.97328319	$0.6624110117 \times 10^{-14}$
−6.918007349	$0.1013547252 \times 10^{-13}$	19.94726277	−2.746755035
−9.255569610	$0.6353108438 \times 10^{-12}$	19.94726277	2.746755035
−9.374280057	3.141592654	19.59502703	$0.3767131383 \times 10^{-12}$
		18.60302016	$-0.8926701053 \times 10^{-12}$
		17.53335984	$-0.9612664776 \times 10^{-12}$
		17.50061768	3.141592654
		17.25850271	2.631904337
		17.25850271	−2.631904337
		16.85734691	$0.7290200442 \times 10^{-12}$
		16.59625463	−1.602085396
		16.59625463	1.602085396
		15.21987519	$-0.1968786492 \times 10^{-11}$
		14.24354652	−3.141592654

[a]The system parameters are the same as in Fig. 1.

the computation time becomes proportional to the total number of layers. In Section 3 we present the fundamentals of the S-matrix algorithm together with several numerical examples and a comparative analysis of computation times.

3. S-Matrix Algorithm

Instead of multiplying the transmission matrices of the consecutive layers, as is done in the T-matrix algorithm, the S-matrix algorithm uses the intermediate transmission matrices to construct the scattering matrix for each slice and then for the entire system. The scattering matrix determines the link between the incident and the scattered amplitudes:

$$\begin{bmatrix} b_n^{(j,+)} \\ b_n^{(0,-)} \end{bmatrix} = \begin{bmatrix} S_{11}^{(j)} & S_{12}^{(j)} \\ S_{21}^{(j)} & S_{22}^{(j)} \end{bmatrix} \begin{bmatrix} b_n^{(0,+)} \\ b_n^{(j,-)} \end{bmatrix}. \tag{24}$$

There are two differences between Eqs. (15) and (24). First, the S matrix links the amplitudes in the jth and the lowest slides (the 0th one), whereas the T matrix links the amplitudes in the consecutive layers. Second, the known (incident) amplitudes are on the right-hand side of Eq. (24), whereas the unknown scattered amplitudes are on the left-hand side; however, they are mixed in Eq. (15). These two differences have proved to be substantial for maintaining the stability of the algorithm, based on Eq. (24). The price that must be paid is that several additional matrix operations must be made to differentiate the S-matrix components from the T-matrix components, by use of the numerical integration of Maxwell equations through each slice. Each block element of $S^{(j)}$ is found from the block elements of $S^{(j-1)}$ and $T^{(j)}$:

$$S_{22}^{(j)} = S_{22}^{(j-1)} Z_{22}^{(j)}, \tag{25a}$$

$$S_{12}^{(j)} = [T_{12}^{(j)} + T_{11}^{(j)} S_{12}^{(j-1)}] Z_{22}^{(j)}, \tag{25b}$$

$$S_{11}^{(j)} = [T_{11}^{(j)} - T_{12}^{(j)} S_{21}^{(j-1)}] S_{11}^{(j-1)}, \tag{25c}$$

$$S_{11}^{(j)} = S_{21}^{(j-1)} - S_{22}^{(j)} T_{21}^{(j)} S_{11}^{(j-1)}, \tag{25d}$$

with

$$Z_{22}^{(j)} = [T_{22}^{(j)} + T_{21}^{(j)} S_{12}^{(j-1)}]^{-1}, \tag{26}$$

and the starting values are $S_{11}^{(0)} = I$, $S_{12}^{(0)} = 0$, $S_{21}^{(0)} = 0$, and $S_{22}^{(0)} = I$, where I is a unit matrix.

As is obvious from Eqs. (25) and (26), it is necessary to calculate the S matrix for a given layer after performing the calculations for all the layers situated below. Thus the computation time will grow with the total number of layers. For identical layers it is possible to store the results for the T matrix obtained with a single numerical integration (the most time-consuming operation) across the layer and then to use them in Eqs. (25) and (26). This could save substantial time, as is evident from Table 2, where a comparison is given for the time consumption with the algorithms based on the T matrix [Eqs. (18)–(23)] approach and on the S-matrix [Eqs. (24)–(26)] approach. The S-matrix results are divided into two cases, those with and without storage of the intermediate T matrix (i.e., numerical integration across all the layers, no matter whether there are identical lay-

Table 2. Comparison of Computation Times (s)

	Number of Layers (M)					
M	7			17		
Number of Layers (N)	10	20	200	10	20	200
With Eq. (23)	1	1	1	Wrong results	Wrong results	Wrong results
S Matrix with storage	4	7	35	35	38	60
S Matrix with integration	8	14	100	50	100	1000

ers). The latter approach could seem useless, but it could be indispensable when the system has nonlinear optical properties.

An important remark concerning the S-matrix algorithm should be made. The algorithm works fairly well when knowledge of the diffraction-order amplitudes is required in the cladding and in the substrate. However, in many cases it is important to know the value of the field inside the structure. At first sight, once the transmitted and reflected amplitudes are known, one can easily determine the amplitudes at the boundaries of each slice by inverting Eq. (24):

$$b_n^{(j,-)} = S_{22}^{(j)-1} b_n^{(1,-)}, \tag{27a}$$

$$b_n^{(j,+)} = S_{12}^{(j)} b_n^{(j,-)}. \tag{27b}$$

However, matrix S_{22} must be inverted at each slice. The problem lies not in the increase of the computation time but rather in the numerical instabilities of this inversion, because the inverse of S_{22} is directly linked with transmission matrix T, which is unstable. To avoid this problem it is necessary to use another connection between field amplitudes, namely,

$$b_n^{(1,-)} = S_{22}^{(N)} b_n^{(N,-)}. \tag{28}$$

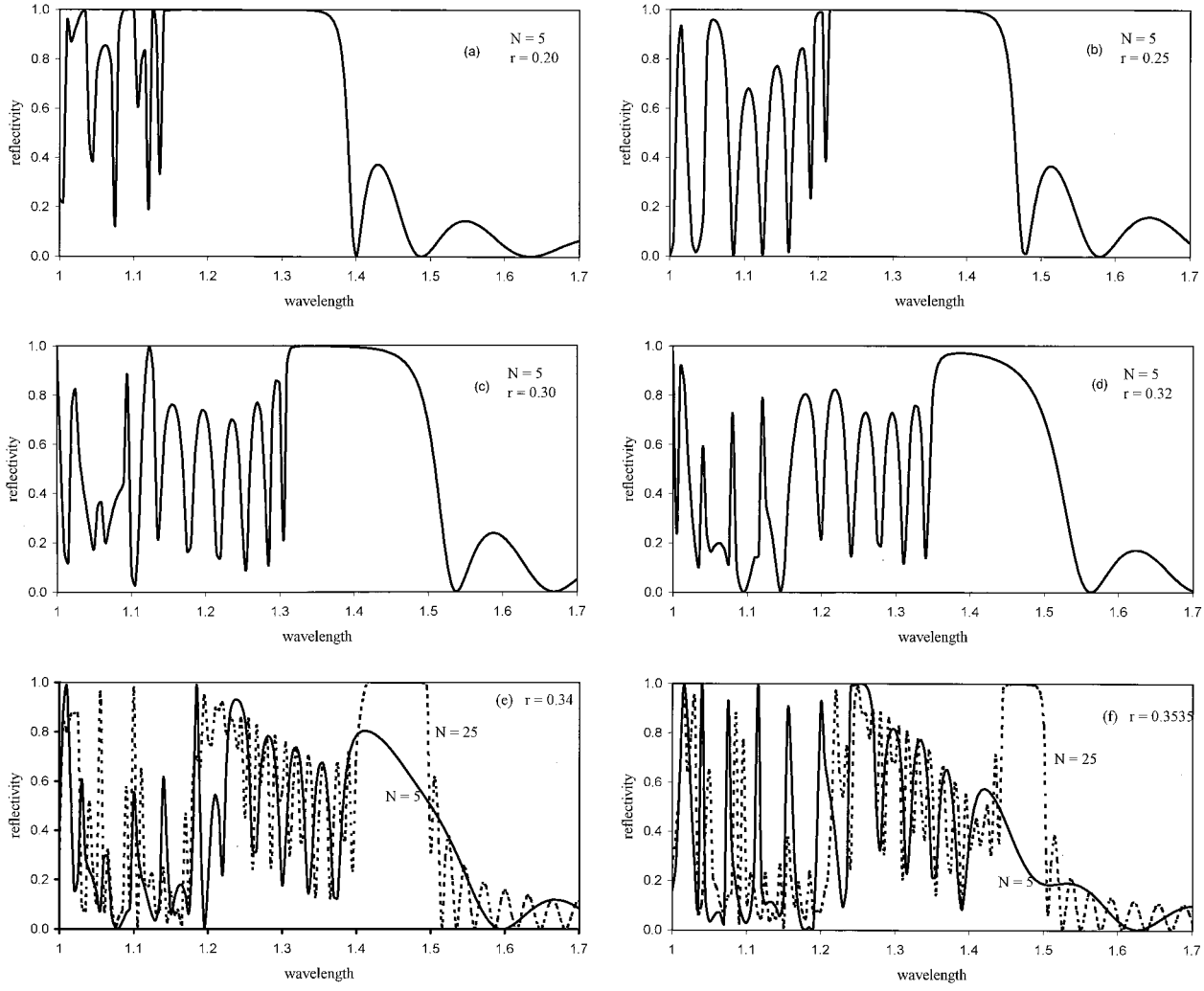

Fig. 3. Reflectivity of a system of circular dielectric rods for 4 rod radii r. $d = h = 1$ μm, $c = 0.5$ μm. $n_1 = 1$, $n_2 = n_3 = 1.5$, normal incidence, TE polarization. Solid curves, $N = 5$; dotted curves, $N = 25$: (a) no interpenetration, (b) the penetration limit. (f) $r = \sqrt{2}/4$; the cylinders in consecutive layers shifted horizontally by c touch one another.

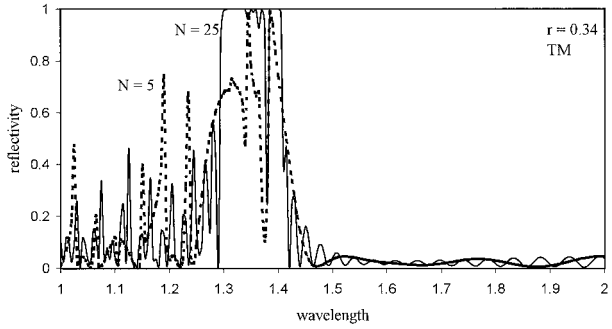

Fig. 4. Reflectivity in TM polarization of a system of dielectric rods. Parameters other than that of r are listed in Fig. 3.

Use of Eqs. (27a), (28), and (25a) gives another expression for $b_n^{(j,-)}$:

$$b_n^{(j,-)} = [Z_{22}^{(j+1)}]^{-1}[Z_{22}^{(j+2)}]^{-1} \ldots [Z_{22}^{(N-1)}]^{-1} b_n^{(N,-)}. \quad (29)$$

It is not necessary to invert the Z_{22} matrices, as their inverse is already known according to Eq. (26), but merely to store them during the integration. We use Eq. (27b) to find the other component, $b_n^{(j,+)}$.

When the field distribution is required inside the slices rather than only on their boundaries, there are two ways to obtain it: either by increasing the number of slices or by further integrating Eqs. (10)–(14) with known shooting amplitudes inside each slice, which causes no numerical problems.

4. Numerical Example

To illustrate the applicability of the method to photonic crystal studies, we give an example that consists of a set of dielectric rods [Fig. 1(a) or Fig. 1(b)] with identical periods in the vertical and horizontal directions ($h = d$) and intermediate rods in the middle ($c = d/2$). Depending on rod radius r, the rod layers either penetrate mutually or do not (r greater or smaller than $d/2$, respectively). First we consider a stack of 11-layer rods ($N = 5$); Fig. 3, solid curves]. For smaller rod radii (r not exceeding $0.3d$), a pronounced bandgap (in transmission) is formed, which shifts toward a longer wavelength and decreases in width with growth of the radius. When the radius increases further (note that at $r = d\sqrt{2}/4$ the cylinders touch one other), the reflection maxima decrease in amplitude and width, probably because of the decrease in contrast (the rod core region becomes increasingly greater than the filling zone area). We can restore the transmission bandgap by increasing the number of rods in the stack, as can be observed for $N = 25$ (i.e., in total, 51 lines of rods in Figs. 3(e) and 3(f); dotted curves).

Figure 4 shows the reflectivity of the system with $N = 5$ and $N = 25$ and radius $r = 0.34$ in TM polarization. Because of the slower convergence rate, it is necessary to double the truncation parameter (39 diffraction orders are taken into account rather than the 17 required for TE polarization).

5. Conclusions

An application of the classic differential method for photonic crystals consisting of arrays of cylindrical elements that are periodic in one direction and quasiperiodic in the other direction has been discussed. Two algorithms were discussed, and their numerical stability and amount of time that they consume were analyzed. The method seems quite useful when there is interpenetration of consecutive elements and for elements of arbitrary geometry. Several numerical examples were presented to illustrate the method.

The authors acknowledge the financial support of the National Fund for Scientific Researches of Bulgaria under contract F714.

References

1. E. Yablonovitch, "Inhibited spontaneous emission in solid-state physics and electronics," Phys. Rev. Lett. **58,** 2059–2062 (1987).
2. S. John, "Strong localization of photons in certain disordered dielectric superlattices," Phys. Rev. Lett. **58,** 2486–2489 (1987).
3. K. Ho, C. Chan, and C. Soukoulis, "Existence of a photonic gap in periodic dielectric structures," Phys. Rev. Lett. **65,** 3152–3155 (1990).
4. P. Villeneuve, Sh. Fan, and J. Joannopoulos, "Microcavities in photonic crystals," in *Microcavities and Photonic Bandgaps*, J. Rarity and C. Weisbuch, eds. (Kluwer Scientific, Dordrecht, The Netherlands, 1996), pp. 133–151.
5. Z. Zhang and S. Satpathy, "Electromagnetic wave propagation in periodic structures: Bloch wave solution of Maxwell's equations," Phys. Rev. Lett. **65,** 2650–2653 (1990).
6. R. Meade, K. Brommer, A. Rappe, and J. Joannopoulos, "Electromagnetic Bloch waves at the surface of a photonic crystal," Phys. Rev. B **44,** 10,961–10,964 (1991).
7. R. Petit, ed., *Electromagnetic Theory of Gratings* (Springer-Verlag, Berlin, 1980).
8. G. Tayeb and D. Maystre, "Rigorous theoretical study of finite-size two-dimensional photonic crystals doped by microcavities," J. Opt. Soc. Am A **14,** 3323–3332 (1997).
9. D. Maystre, "Electromagnetic study of photonic band gaps," Pure Appl. Opt. **3,** 975–993 (1994).
10. F. Wijnands, J. Pendry, P. Roberts, P. Bell, L. Moreno, and F. Garcia-Vidal, "Numerical method for calculating spontaneous emission rate near a surface using Green's functions," in *Microcavities and Photonic Bandgaps*, J. Rarity and C. Weisbuch, eds. (Kluwer, Scientific, Dordrecht, The Netherlands, 1996), pp. 299–308.
11. P. Dansas and N. Paraire, "Fast modeling of photonic bandgap structures by use of a diffraction-grating approach," J. Opt. Soc. Am. A **15,** 1586–1598 (1998).
12. F. Montiel and M. Neviere, "Differential theory of gratings: extension to deep gratings of arbitrary profile and permittivity through the R-matrix propagation algorithm," J. Opt. Soc. Am. A **11,** 3241–3250 (1994).
13. E. Loewen and E. Popov, *Diffraction Gratings and Applications* (Marcel Dekker, New York, 1997).
14. E. Popov, B. Bozhkov, D. Maystre, and J. Hoose, "Integral method for echelles covered with lossless or absorbing thin dielectric layers," Appl. Opt. **38,** 47–55 (1999).
15. M. G. Moharam and T. K. Gaylord, "Rigorous coupled-wave analysis of dielectric surface-relief gratings," J. Opt. Soc. Am. **72,** 1385–1392 (1982).
16. L. Li, "Formulation and comparison of two recursive matrix algorithms for modeling layered diffraction gratings," J. Opt. Soc. Am. A **13,** 1024–1035 (1996).